INVESTIGATION OF RECONSTRUCTIVE OPERATORS FOR COMPTON-SCATTERING TOMOGRAPHY

MICHAEL THRAMANN

1. Introduction

In this project I designed, tested, and analyzed backprojective and reconstruction operators for Compton-Scattering Tomography. First, I generated data representative of such scans, and then coded-up and ran different reconstruction operators. I then compared the produced images, sought mathematical explanations for my results, and consulted with my advisor, Todd Quinto. With his feedback, I iterated on previous attempts to try to eliminate numerical noise and reconstructive artifacts. While I wasn't always completely successful, I did make progress, and in some cases improved on traditional methods of reconstruction.

For simplicity, I considered a two dimensional case: analogous to slices of a three dimensional scan. The reconstructive characteristics observed in a plane are informative for those of scans in three dimensions. Projected into two dimensions, the scanner shape is naturally a pair of rays originating from a vertex[1]. Three dimensional cone scans are simply integrals over rotations of this two dimensional projection. Another simplification I made was to consider my scanned media to be the unit disc:

$$D(x,y) = \begin{cases} 1, & x^2+y^2 \leq 1 \\ 0, & x^2+y^2 > 1 \end{cases} \tag{1}$$

Still, I took considerations so that my reconstructions would generalize to more complex shapes.

The project was segmented into three phases, each investigating different backprojection methods (and none at all). These different methods were a result of holding different cone characteristics constant. This is further explained in *Defining the Cone* and *The Necessity of Changing Cone Variables*.

I ultimately identified a near-successful reconstruction technique for the first scenario, and demonstrated parallels in methods for reducing artifacts between the second scenario and limited angle tomography. A shallow analysis of the third scenario also built intuition for higher dimensions.

All of my work on this project was dependent on Professor Quinto's guidance, with exception of the actual grunt work of coding and pursuing certain reconstructions. I am greatly appreciative of the introduction to tomography, and his facilitation of my first steps into the world of inverse problems.

1.1. Defining the Cone.

The cone in Figure 1 is representative of the cone that I used to generate all of my data. The vertex of the cone is (x_0, y_0), θ is the angle between the lines and the centerline (i.e. half of the width of the cone), and ϕ is the tilt of the cone measured from the centerline to horizontal. To eliminate redundancy, θ is restricted to the interval $[0, \pi/4]$.

Initially, I evaluated the integrals of the media over the cone, by building a parameterized function (Equation 2).

[1]Because of this inheritance, this report will refer to these lines as a cone.

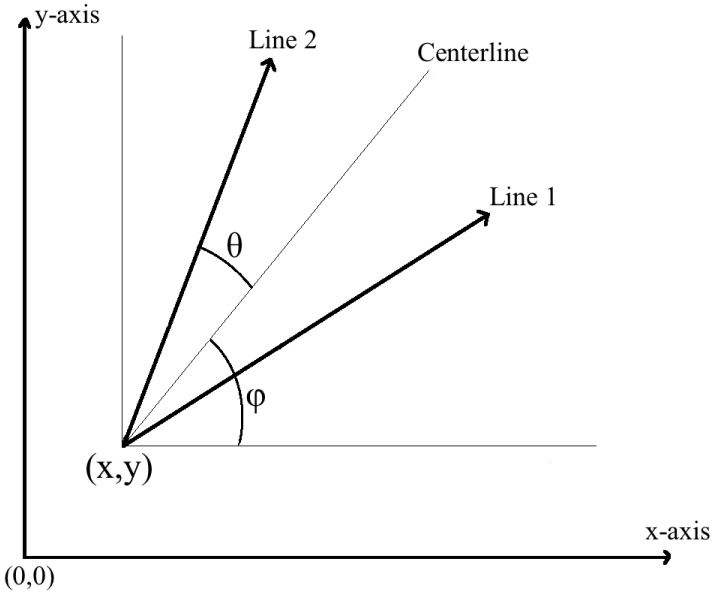

FIGURE 1. Picture of 2D scanning cone.

$$T(l) = \overbrace{D(x + l\cos(\phi - \theta), y + l\sin(\phi - \theta))}^{\text{Line 1}} + \overbrace{D(x + l\cos(\phi + \theta), y + l\sin(\phi + \theta))}^{\text{Line 2}} \tag{2}$$

Note that the parameter l is the length along the lines. I then numerically integrated over $T(l)$ to obtain data for a given $(x, y), \phi$, and θ.

After some use of this method, however, I deduced that the numerical integration was producing unnecessary noise. I first attempted to dampen this noise by averaging the data's samples over different regions. While this worked mildly well, I then moved on to perform the integration analytically. This eliminated any non-reconstructive error (and fortuitously decreased the runtime of my calculations).

1.2. **The Necessity of Changing Cone Variables.** In the three scenarios which I investigated, I always varied two aspects of the cone (out of x, y, ϕ, and θ), while holding the others constant. This dimensionality is necessary to build accurate reconstructions; it is very easy to conjure up examples of media that foil scans that only vary in one dimension.

1.3. **The Three Cases.** In Section 2, (x, y) of the cone were my variables, while I held θ and ϕ constant. I varied (x, y) on the ranges $-2 \leq x \leq 2, -2 \leq y \leq 2$.

In Section 3, x and θ of the cone were my variables, while I held y and ϕ constant. I experimented with different ranges of varying x, but eventually stuck with $-10 \leq x \leq 10$. And θ varied over $[0, \pi/2]$.

And in Section 4, x and ϕ of the cone were my variables, and I held y and θ constant. I varied x over $[-10, 10]$ and ϕ over $[-\theta, \theta]$.

2. Varying Cone Position at Constant Size and Tilt

For this first scenario, I varied the (x, y) position of the cone, while maintaining a constant θ and ϕ. This made it very easy to build image-like representations of the data; simply evaluate *The*

Scanning Function at every point corresponding to a pixel. In fact, the density of these points is of large consequence during the reconstruction phase.

2.1. **The Scanning Function.** The following function was evaluated at every point over a grid containing the unit disc (specifically, $-2 \leq x \leq 2, -2 \leq y \leq 2$).

$$V(x,y) = \int_0^\infty \underbrace{D(x + l\cos(\phi_0 - \theta_0), y + l\sin(\phi_0 - \theta_0))}_{\text{Line 1}} + \underbrace{D(x + l\cos(\phi_0 + \theta_0), y + l\sin(\phi_0 + \theta_0))}_{\text{Line 2}}\, dl \tag{3}$$

This then created an image of the scanning data, on which I could perform reconstructive operators.

2.2. **Cone Lines Along Axes.** At first, I considered the simplest case, where $\theta_0 = \pi/4, \phi_0 = \pi/4$. This case is simple because both lines lie along the x and y axes. Upon seeing the data, it was clear that a derivative would be most effective for reconstruction. My intuition led me to integrate over x, and then y, like so

$$A(x,y) = \frac{\partial^2 V(x,y)}{\partial y \partial x} \tag{4}$$

Another operator for this simple case is just derivation twice by x:

$$A(x,y) = \frac{\partial^2 V(x,y)}{(\partial x)^2} \tag{5}$$

Figure 2 shows the collected data, and each of the above reconstructions.

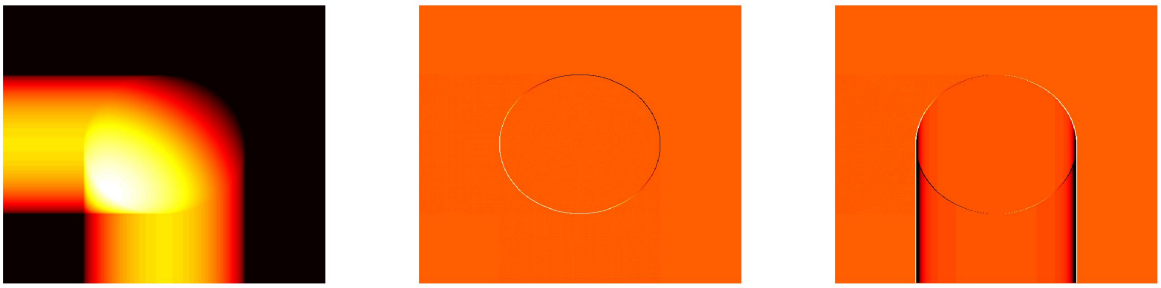

FIGURE 2. From L to R: Data generated from scanner, Reconstruction via Equation 4, Reconstruction via Equation 5.

Notice that Equation 5 produces artifact streaks tangent to the disc, while Equation 4 does not. In fact, this method has very few artifacts, and clearly shows the outline of the disc. Still, this result is less interesting. Looking at the scanner data, it is easy to see why a compound derivative in the axis directions will lead to a perfect outline.

The more interesting result is the artifacts in the third image in Figure 2. The reasoning for these lines is further investigated and described in Section 2.4.

2.3. **Other Cone Sizes and Tilts.** Although the above work was informative, it really only addresses a very niche case of data collection. I pursued more general results by choosing an arbitrary set of constant angles that yielded lines not parallel to the axes. In fact, for most of my analysis I took $\theta_0 = \pi/6$ and $\phi_0 = \pi/2$.

For this set-up, I tried many different reconstruction operators, and the fewest artifacts came from an extension of Equation 4:

$$\bigtriangledown_{\phi-\theta} = \frac{\partial}{\partial x}\cos(\phi-\theta) + \frac{\partial}{\partial y}\sin(\phi-\theta) \tag{6}$$

$$\bigtriangledown_{\phi+\theta} = \frac{\partial}{\partial x}\cos(\phi+\theta) + \frac{\partial}{\partial y}\sin(\phi+\theta) \tag{7}$$

This composition, $\bigtriangledown_{\phi-\theta}\bigtriangledown_{\phi+\theta}(V)$, is just deriving over each of the cone lines with directional derivatives. My other notable attempt was using the Laplacian operator:

$$\bigtriangledown^2 = \frac{\partial^2}{(\partial x)^2} + \frac{\partial^2}{(\partial y)^2} \tag{8}$$

These reconstructions are depicted in Figure 3.

2.4. **Explanation of Observed Artifacts.** Clearly, these observed artifacts are primarily streaks tangent to the circle along Line 1 and Line 2. And I saw the same pattern before with the second derivative with respect to x. The reason these artifacts occur is because these derivatives are over a discrete grid, where the direction of the derivatives is not parallel to the direction of the partitions. Therefore, the derivatives are inexact approximations.

In fact, as this grid gets more refined (i.e. the mesh of the partition gets smaller), the scale of the artifacts decreases (see Figure 4).

Of course, so does the size of the boundary of the disc. With more time, possible areas of exploration may include different methods of regressing over the the grid points and taking continuous derivatives, or using rotational transformations to map points in a tilted grid to the vertical and horizontal axes of an image. The latter method would include the added challenge of different rotations for each line, as the lines are not always perpendicular.

However, it is interesting to note that each set of artifacts is unique to the size and tilt of the cone, while the depiction of the disc boundary is not. This suggests that varying the cone angles, instead of its (x, y) position, is a promising reconstruction method.

3. Varying Cone Width and Horizontal Position

In this part of the project, I set $y_0 = -2, \phi_0 = \pi/2$ as constants, while I varied x and θ. Building useful image data out of this variation is less intuitive than the case of changing position.

3.1. **The Backprojector Function.** Note that given a point (x_1, y_1) in the image, and an x coordinate for the cone vertex (and the previously stated constants), there exists an angle θ such that one of the cone lines goes through that point in the image:

$$\theta(x, (x_1, y_1)) = \arctan\left(\frac{x - x_1}{y_1 - y_0}\right) \tag{9}$$

It is then easy to write a function, $\overline{V}$, that given every point in the image, returns the integral of every cone scan through that point, with respect to changes in the x of the cone's vertex. It is

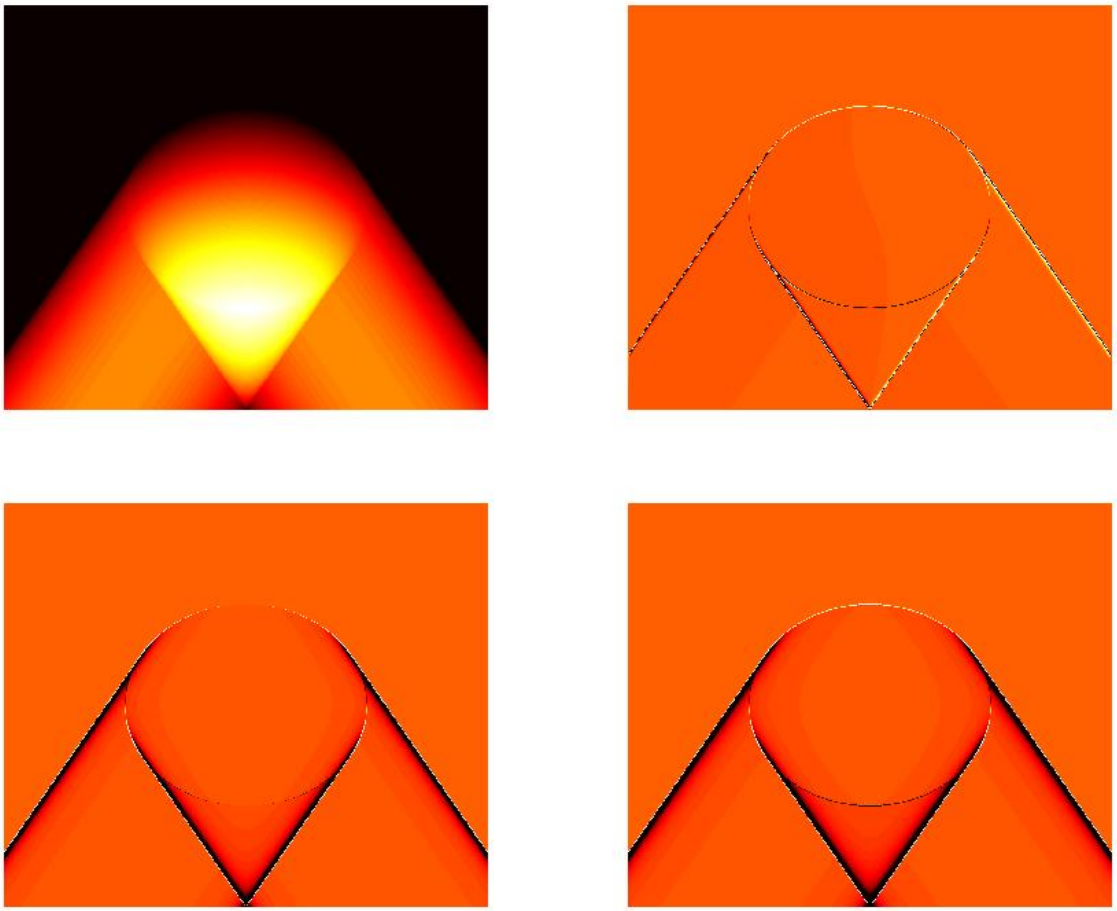

FIGURE 3. Clockwise from top left: Scanner data, Reconstruction from Equations 6 and 7, Reconstruction from Equation 8, Reconstruction from Equation 5.

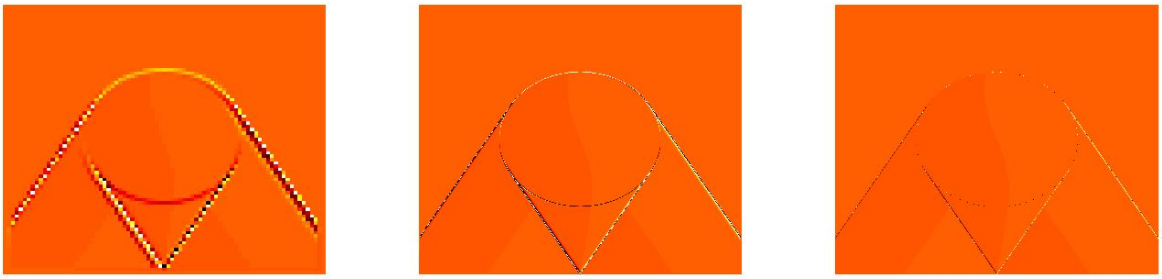

FIGURE 4. L to R: 80x80 reconstruction, 800x800 reconstruction, 8000x8000 reconstruction

also important to consider that I needed to bound the interval over which I integrated. For now, consider this interval $[-a, a]$, where a is a positive real number.

$$\overline{V}(x,y) = \int_{-a}^{a}\int_{0}^{\infty} D(x + l\cos(\phi_0 - \theta(x)), y_0 + l\sin(\phi_0 - \theta(x))) + D(x + l\cos(\phi_0 + \theta(x)), y_0 + l\sin(\phi_0 + \theta(x)))\, dl\, dx \tag{10}$$

3.2. **Explaining Artifacts from Initial Scans.** From my first reconstructions, it was apparent that the chosen a had a large effect on reconstructive artifacts (see Figure 5). At this stage, I chose to use the Laplace operator from Equation 8 because it was the best performing "line naive" operator. Also note that the outer integral over x was performed numerically, and led to numerical error (particularly evident near the bottom of the images).

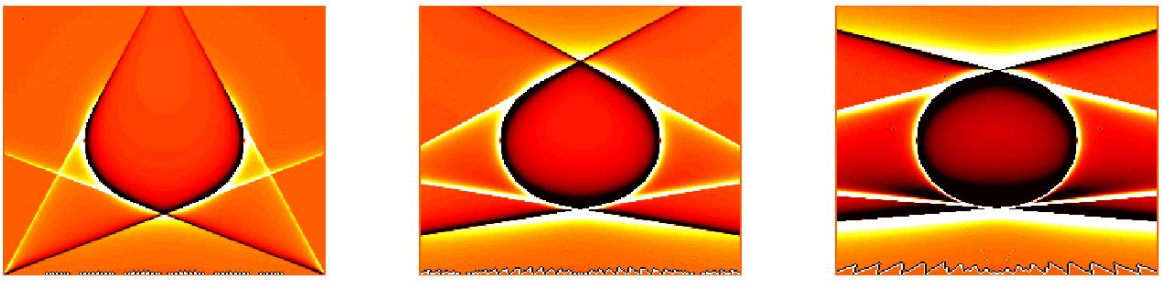

FIGURE 5. L to R: a = 2 reconstruction, a = 5 reconstruction, a = 10 reconstruction

3.3. **Weighting the Scans over the Interval.** Of course, the reconstructive artifacts are still largely tangent lines to the circle. These lines are the scan lines for when the scanner vertex is at the extrema of the interval $[-a, a]$. My intuition led to me to try a larger a, but give greater weight to the scans near the media. I first used the following function:

$$W(x) = \frac{(a - |x|)}{a} \tag{11}$$

Professor Quinto then recommended that I instead try continuously differentiable functions, so as to minimize false singularities in the backprojection phase. In fact, a similar problem had come up in his previous work on limited angle tomography [1], so I adapted one of his functions from the limited-angle case to the limited-range of the x coordinate case:

$$W(x) = e^{\left(\frac{x^2}{x^2 - a^2}\right)} \tag{12}$$

I also tried using a normal distribution centered at 0, with different standard deviations:

$$W(x) = \frac{1}{\sigma\sqrt{2\pi}} e^{\frac{-(x^2)}{2\sigma^2}} \tag{13}$$

Lastly, I tried a trigonometric function:

$$W(x) = \frac{1}{2}(cos\left(\frac{x}{\pi}\right) + 1) \tag{14}$$

Figure 6 compares the different reconstruction results for the different weighting methods. I took $a = 10$ and $\sigma = 4$.These four images are all at equal color scaling and resolution.

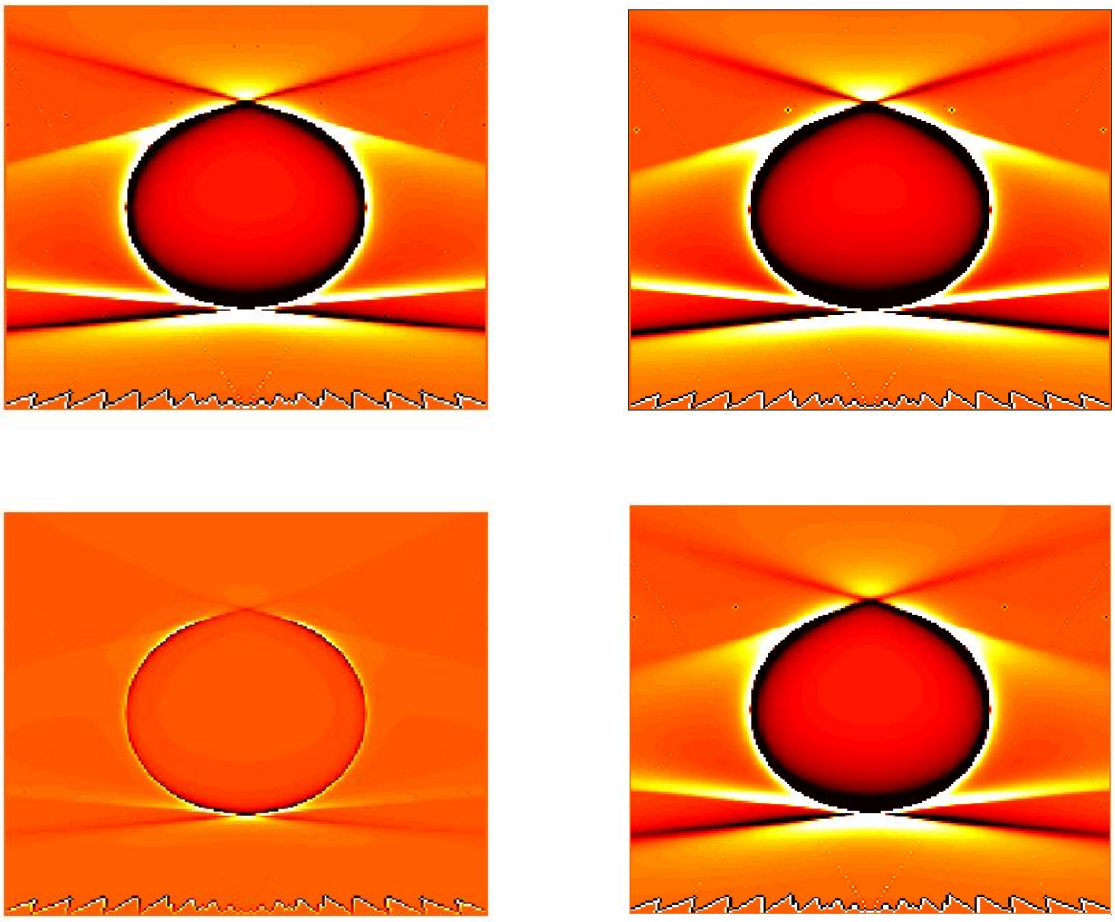

FIGURE 6. Clockwise from top left: Equation 11 reconstruction, Equation 12 reconstruction, trigonometric wave reconstruction (Equation 14), normal distribution reconstruction (Equation 13).

3.4. **Trade-offs in Weighting Scans.** Perhaps the most obvious difference is that the normal distribution reconstruction is scaled less dramatically than the others. This is less consequential than it may appear to be; each of these weight functions has different areas under their curves, and thus scales the whole color spectrum of the image differently. For example, the area under the normal distribution is 1, while the area under Equation 14 is ~ 9.87, almost a whole order of magnitude. It would be very simple to rescale one or the other to appear standardized.

The real tradeoff, however, lies in how quickly the weight function falls off as it approaches the bounds of integration. Should the function decrease only very close to the end, it will not greatly reduce the presence of tangential artifacts, and more likely just change their angle slightly to resemble a smaller domain of integration. Should the function decrease very soon, however, the reconstruction will less accurately represent the media.

Naturally, this decision should be made by considering what information is already known. If artifacts will be easily distinguishable from the media, but the media itself is not already well-defined in shape, it makes sense to use a more abrupt and sharper fall-off for $W(x)$. Likewise, if

the media's shape is well-known, but artifacts will be less distinguishable, one should consider a $W(x)$ with a more gradual decrease.

4. Varying Cone Tilt and Horizontal Position

For this third and final scenario, I held $y_0 = -2$ and $\theta_0 = \pi/4$ constant, while varying x and ϕ. The backprojection for this scenario is very similar to the second scenario above.

4.1. **The Backprojector Function.** Given a point (x_1, y_1) in the image, and an x coordinate for the cone vertex (and the new constants), there now exists either one or two ϕ's such that one of the cone lines goes through that point in the image. To simplify the data, we restrict ϕ to $[-\pi/4, \pi/4]$. This way, there always exists solely one ϕ for a point (x_1, y_1):

$$\phi(x,(x_1,y_1)) = \begin{cases} \theta_0 + \arctan\left(\frac{y_1}{x-x_1}\right), & x \le 0 \\ \pi - \theta_0 - \arctan\left(\frac{y_1}{x-x_1}\right), & x > 0 \end{cases} \tag{15}$$

Much as in the second case, it is now easy to create a function to collect necessary data:

$$\begin{aligned} \ddot{V}(x,y) = \int_{-a}^{a}\int_{0}^{\infty} & D(x + l\cos(\phi(x) - \theta_0), y_0 + l\sin(\phi(x) - \theta_0)) + \\ & D(x + l\cos(\phi(x) + \theta_0), y_0 + l\sin(\phi(x) + \theta_0))\, dl\, dx \end{aligned} \tag{16}$$

4.2. **The Reconstructions.** And as one might expect, the data and reconstructions of this third scenario very closely resemble those of the second scenario, albeit with slightly different artifacts (mostly from the numerical integration):

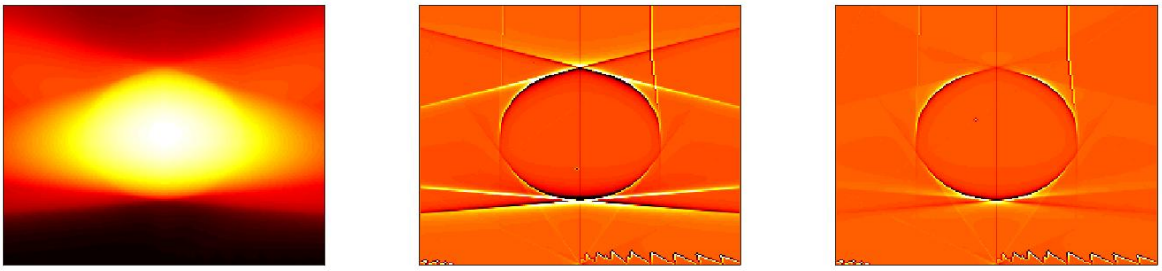

Figure 7. From L to R: Scenario 3 data, Reconstruction with Laplacian Operator (Equation 8), Reconstruction with normal distribution weights and Laplacian Operator (Equations 13 and 8).

With more time, one might investigate if weighting is another effective method to produce better scans, and if the tradeoff described in Section 3.4 is either better or ill-posed to help in this third scenario.

References

[1] Jrgen Frikel and Eric Todd Quinto. Characterization and reduction of artifacts in limited angle tomography. *Inverse Problems*, 29:11, 2013.

Department of Mathematics
Tufts University, Medford, MA, USA
E-mail address: michael.thramann@tufts.edu